Unsteady Thermal Boundary Layer Flows of a Bingham Fluid in a Porous Medium following a sudden change in surface heat flux

D. Andrew S. Rees[(1)], **Andrew P. Bassom**[(2,3)]

[(1)] *Department of Mechanical Engineering, University of Bath, Bath BA2 7AY, U.K.*

[(2)] *School of Mathematics and Statistics, The University of Western Australia, Crawley WA 6009, Australia*

[(3)] *School of Mathematics and Physics, University of Tasmania, Private Bag 37, Hobart, TAS 7001, Australia (permanent address)*

✉ D.A.S.Rees@bath.ac.uk, andrew.bassom@uwa.edu.au

Abstract We consider the effect of suddenly applying a uniform heat flux to a vertical wall bounding a porous medium which is saturated by a Bingham fluid. We consider both an infinite porous domain and a vertical channel of finite width. Initially, the evolving temperature field provides too little buoyancy force to overcome the yield threshold of the fluid. For the infinite domain convection will always eventually arise, but this does not necessarily happen in the vertical channel. We show (i) how the presence of yield surfaces alters the classical results for Newtonian flows and (ii) the manner in which the locations of the yield surfaces change as time progresses.

Keywords Porous media · Boundary layer · Unsteady flow · Convection · Bingham fluid · Yield stress

Nomenclature

Latin letters

$\mathcal{D}$	equal to $\ln \delta$
$F(\mathrm{Rb})$	location of the yield surface
g	gravity
G	threshold body force
K	permeability
L	length scale
p	pressure
p_x	pressure gradient in the x-direction
Q	total vertical velocity flux
Ra	Darcy-Rayleigh number
Rb	Rees-Bingham number
t	time
T	temperature (dimensional)
T_0	ambient (cold) temperature
T_1	temperature of heated surface
u	vertical Darcy velocity
x	vertical coordinate
y	horizontal coordinate
z	dummy variable

Greek letters

α	thermal diffusivity
β	coefficient of cubical expansion
η	similarity variation
η_{y}	location of yield surface
θ	temperature (nondimensional)
μ	dynamic viscosity
ρ	reference density
σ	heat capacity ratio

Other symbols

$\bar{}$	dimensional quantities

1 Introduction

Bingham fluids are an example of a yield stress fluid. Unlike Herschel-Bulkeley and Casson fluids, they exhibit a linear stress-strain relationship once the yield stress is exceeded. They arise in a wide variety of situations both in the environment and industry, and examples of the very many natural and man-made fluids which exhibit a yield stress have been collated and prsented in the chapter [1].

The aim of the present short paper is to investigate the manner in which convection arises when a Bingham fluid saturates a porous medium. There already exist some papers on this type of topic, but they are concerned with the equivalent fluid problem, i.e. there is no porous matrix present. We refer to the analyses

by Yang and Yeh [2] and Bayazitoglu et al. [3] who studied free convection in a sidewall-heated channel. They find that steady convection will only arise whenever the Rayleigh number is sufficiently large that the buoyancy force is then able to overcome the yield stress. When flow occurs the velocity profile consists of five regions, with three regions of flow alternating with two of plug flow (i.e. constant velocity with no shear). The plug flow regions are themselves moving and are placed at equal distances either side of the centreline of the channel. Other papers which consider variations on this theme are those by Patel and Ingham [4] who consider a mixed convection with the combination of buoyancy and a driving pressure gradient, Barletta and Magyari [5] who consider a free convection variant on vertical Couette flow, and Karimfazli and Frigaard [6] whose study of free convection when the boundary temperatures vary linearly with distance up the walls. The unsteady analysis of Kleppe and Marner [7] is also important because it considers the evolution of the temperature and velocity profiles in a vertical channel after an sudden change in temperature of one of the vertical walls.

The present paper considers the unsteady unidirection convection which is set up by suddenly changing the boundary heat flux of a vertical surface. This is a natural extension to the work of Rees and Bassom [8] who studied an impulisive change in the boundary temperature. We will see that the final outcome here has many qualititative differences from those found in [8]. Again, we will consider both a semi-infinite domain (i.e. bounded by a single vertical wall), and a vertical channel of constant thickness. As in [8] buoyancy forces spread into the porous medium due to the diffusion of heat from the heated surface. We find that convection does not happen at first, but that there is an onset time after which convection persists. We present detailed exact solutions for the locations of the yield surfaces and overall velocity flux, and an asymptotic analysis yields highly accurate data for large times.

2 Governing Equations

We follow the early paper by Pascal [X] which employed a threshold gradient model to model the one-dimensional flow of a Bingham fluid in a porous medium:

$$\overline{u} = \begin{cases} -\dfrac{K}{\mu}\Big[1 - \dfrac{G}{|\overline{p}_{\overline{x}}|}\Big]\overline{p}_{\overline{x}} & \text{when } |\overline{p}_{\overline{x}}| > G, \\ 0 & \text{otherwise,} \end{cases} \tag{1}$$

where G denotes the threshold gradient (or, more generally, the threshold body force) above which the fluid yields. When buoyancy is included as an extra body force, the threshold model becomes,

$$\overline{u} = \begin{cases} -\dfrac{K}{\mu}\left[1 - \dfrac{G}{|\overline{p}_{\overline{x}} - \rho g\beta(T - T_0)|}\right]\Big(\overline{p}_{\overline{x}} - \rho g\beta(T - T_0)\Big) & \text{when } |\overline{p}_{\overline{x}} - \rho g\beta(T - T_0)| > G, \\ 0 & \text{otherwise,} \end{cases} \tag{2}$$

where $\overline{x}$ is now the vertical coordinate and $\overline{u}$ is the corresponding Darcy velocity. We have assumed that the Boussinesq approximation applies when writing down the buoyancy term, and T_0 is the initial temperature of the porous medium. If a heated vertical surface is of infinite extent in both the positive and negative $\overline{x}$-directions, then there will be no horizontal fluid velocity, and therefore $\overline{v} = 0$. We may allow both $\overline{u}$ and T to be functions only of the horizontal coordinate, $\overline{y}$, and time, $\overline{t}$, and so the equation of continuity is satisfied and the heat transport equation is,

$$\sigma T_{\overline{t}} = \alpha T_{\overline{y}\,\overline{y}}, \tag{3}$$

where σ is heat capacity ratio between the porous medium and the saturating fluid, and α is the thermal diffusivity of the porous medium. At $\overline{t} = 0$ a uniform and steady heat flux, q, is applied to the vertical bounding surface:

$$k\frac{\partial T}{\partial \overline{y}} = -q, \tag{4}$$

where k is the thermal conductivity of the medium.

Equations (2) and (3) may be nondimensionalised using the scalings,

$$(\overline{x},\overline{y}) = L(x,y), \quad \overline{u} = \frac{\alpha}{L}u, \quad \overline{p} = \frac{\alpha\mu}{K}p, \quad T = T_0 + \frac{qL}{k}\theta, \quad \overline{t} = \frac{\sigma L^2}{\alpha}t, \quad G = \frac{\alpha\mu}{KL}\mathrm{Rb}, \tag{5}$$

and we obtain,

$$u = \begin{cases} \mathrm{Ra}\,\theta - p_x - \mathrm{Rb}, & \mathrm{Rb} < \mathrm{Ra}\,\theta - p_x, \\ 0, & -\mathrm{Rb} < \mathrm{Ra}\,\theta - p_x < \mathrm{Rb}, \\ \mathrm{Ra}\,\theta - p_x + \mathrm{Rb}, & \mathrm{Ra}\,\theta - p_x < -\mathrm{Rb}, \end{cases} \tag{6}$$

and

$$\theta_t = \theta_{yy}. \tag{7}$$

In the above the Darcy-Rayleigh number is given by

$$\mathrm{Ra} = \frac{\rho g \beta q K L^2}{k\mu\alpha}, \tag{8}$$

and the parameter,

$$\mathrm{Rb} = \frac{KL}{\mu\alpha}G. \tag{9}$$

This latter parameter is a scaled version of the yield pressure gradient, G, and might be referred to as a porous convective Bingham number; hereinafter it is termed the Rees-Bingham number.

The lengthscale, L, which was introduced in Eq. (5), will be taken to be the dimensional width of the vertical channel when that configuration is being studied. But when the porous medium occupies a semi-infinite domain there is no natural external lengthscale that may be used. Therefore we set the Darcy-Rayleigh number to a unit value, which will then automatically define a natural lengthscale, L, in terms of the properties of the medium; thus we have,

$$L = \frac{\mu\alpha}{\rho g \beta (T_1 - T_0) K}. \tag{10}$$

The initial condition in nondimensional form is simply that $\theta = 0$ at $t = 0$. For both the infinite domain and the vertical channel we have $\partial\theta/\partial y = -1$ at $y = 0$, whereas we have $\theta \to 0$ as $y \to \infty$ for the infinite domain, and either $\theta = 0$ at $y = 1$ (case (i)) or $\partial\theta/\partial y = 0$ at $y = 1$ (case (ii)) for the vertical channel.

3 The semi-infinite domain

We consider first the heat transfer and flow which is caused by suddenly imposing a unit heat flux to the vertical bounding surface at $y = 0$, i.e. the boundary condition,

$$\frac{\partial\theta}{\partial y} = -1, \tag{11}$$

applies there, and we expect that $\theta \to 0$ as $y \to \infty$. As has already been discussed we are setting $\mathrm{Ra} = 1$ in this semi-infinite case.

Equation (7) for θ is well-known to possess a self-similar solution of the form,

$$\theta = t^{1/2} f(\eta) \qquad \text{where} \qquad \eta = \frac{y}{2\sqrt{t}}, \tag{12}$$

and where

$$f'' + 2\eta f' = 2f, \qquad f'(0) = -1, \qquad f \to 0 \quad \text{as} \quad \eta \to \infty. \tag{13}$$

The solution is

$$f = 2\,\mathrm{ierfc}\,\eta = 2\int_\eta^\infty \mathrm{erfc}\,\xi\, d\xi = \frac{2}{\sqrt{\pi}}e^{-\eta^2} - 2\eta\,\mathrm{erfc}\,\eta, \tag{14}$$

and this profile is shown in Fig. 1.

When the domain is infinite this developing thermal field will generate only upward flows, and therefore the hydrostatic gradient, p_x, which is seen in Eq. (6), must take zero values when one considers conditions in the ambient medium. Therefore Eq. (6) simplifies to,

$$u = \begin{cases} \theta - \mathrm{Rb} & \text{when } \mathrm{Rb} < \theta \\ 0 & \text{when } \theta < \mathrm{Rb}. \end{cases} \tag{15}$$

From this we see that flow arises only when θ takes values which are above Rb. Therefore there will always be an interval of time during which no flow is induced. Given that, at any instant of time, the highest temperature in the domain is at $\eta = 0$, Eq. (14) shows that the time at which convection begins is when $t^{1/2} f(0) = \mathrm{Rb}$, or

$$t = \frac{\pi \mathrm{Rb}^2}{4}. \tag{16}$$

At later times convection takes place in the near-surface sublayer of the thermal boundary layer and there is no motion outside of the yield surface where $\theta = \mathrm{Rb}$. If we denote the location of this yield surface by η_{y}, then

$$\frac{2}{\sqrt{\pi}} e^{-\eta_{\mathrm{y}}{}^2} - 2\eta_{\mathrm{y}} \operatorname{erfc} \eta_{\mathrm{y}} = \frac{\mathrm{Rb}}{\sqrt{t}}. \tag{17}$$

The variation of η_{y} with t/Rb^2 is shown in Fig. 2.

We may now determine the total velocity flux as a function of both Rb and time. First we let,

$$t = \mathrm{Rb}^2 \tau, \tag{18}$$

and therefore the total velocity flux is now given by

$$Q = \int_0^\infty u \, dy = 2\sqrt{\tau}\, \mathrm{Rb} \int_0^{\eta_{\mathrm{y}}} \mathrm{Rb}\Big[\sqrt{\tau} f(\xi) - 1\Big] \, d\xi = \mathrm{Rb}^2 \tau \operatorname{erf} \eta_{\mathrm{y}} = t \operatorname{erf} \eta_{\mathrm{y}}. \tag{19}$$

Given that Q/t is a function solely of η_{y} which is, in turn, a function of τ, we display the variation of Q/t with $\log_{10} 4\tau/\pi$ in Figure 3. Convection begins when $\tau = \pi/4$, and the curve given in Fig. 3 may also be interpreted as the total velocity flux compared with that of a Newtonian fluid.

4 The vertical channel

We now consider convection within a tall cavity with unit nondimensional width, and therefore the Darcy-Rayleigh number now appears as a parameter, as discussed earlier. As in Rees and Bassom [*] we assume that the flow, when it arises, will be parallel and dependent solely on y and t; there will exist turning regions at the upper and lower extremities of the channel within which there will be further x-dependence. One major consequence of this is that there is now no mean flow up the cavity at any time.

Beginning with $\theta = 0$ everywhere, heat transport is induced by suddenly imposing $\theta_y = -1$ on $y = 0$. We will consider two cases corresponding to the following boundary conditions on the second wall:

$$\left.\begin{array}{ll} \text{Case 1:} & \theta = 0 \\ \text{Case 2:} & \theta_y = 0 \end{array}\right\} \quad \text{on } y = 1. \tag{20}$$

Case 1 corresponds to maintaining the right hand wall at the original ambient temperature and therefore one would expect the temperature eventually to tend towards a steady state. On the other hand, Case 2 admits no heat loss, and therefore the mean temperature of the channel will rise linearly in time.

The two respective solutions of (7) are found using a Laplace transform in time; we find that,

$$\text{Case 1:} \qquad \theta = \sum_{n=0}^{\infty} 2t^{1/2} (-1)^n \Big[\operatorname{ierfc}\Big(\eta + \frac{n}{\sqrt{t}}\Big) - \operatorname{ierfc}\Big(\frac{n+1}{\sqrt{t}} - \eta\Big)\Big], \tag{21}$$

$$\text{Case 2:} \qquad \theta = \sum_{n=0}^{\infty} 2t^{1/2}\Big[\text{ierfc}\left(\eta + \frac{n}{\sqrt{t}}\right) + \text{ierfc}\left(\frac{n+1}{\sqrt{t}} - \eta\right)\Big], \tag{22}$$

When $t \ll 1$ it is clear that these two solutions reproduce (14) corrsponding to the infinite domain because the thermal boundary layer is very thin at such early times.

Some temperature profiles at selected times are shown in Figures 4 and 5. For both cases the early-time solutions display the ierfc profile which grows in amplitude with time. For Case 1 (Fig. 4) the evolution towards the ultimate state where

$$\theta = 1 - y \tag{23}$$

is essentially complete by $t = 2$. For Case 2 (Fig. 5) the final state is

$$\theta = t + \tfrac{1}{2}y^2 - y + \tfrac{1}{3}, \tag{24}$$

and the exact profile at $t = 0.5$ is seen to have a very small error; the dotted lines in Fig. 5 depict the asymptotic state.

It is necessary now to determine conditions under which convection will occur. At sufficiently early times the fluid remains stagnant because insufficient heat has passed into the channel and buoyancy forces are too weak. Bearing in mind the form of (6), incipient convection must correspond to

$$\text{Ra}\,\theta_{\max} - p_x = \text{Rb} \qquad \text{and} \tag{25}$$

and

$$\text{Ra}\,\theta_{\min} - p_x = -\text{Rb}. \tag{26}$$

Therefore convection arises when

$$\theta_{\max} - \theta_{\min} = 2\frac{\text{Rb}}{\text{Ra}}, \tag{27}$$

and the corresponding hydrostatic pressure gradient is

$$p_x = \frac{\text{Ra}(\theta_{\max} + \theta_{\min})}{2}. \tag{28}$$

As noted in Rees and Bassom (2014) a zero net upward fluid flux cannot be sustained by allowing p_x to be zero for all time, as is the case for the infinite domain, and therefore the value of p_x must vary in time in order to maintain the zero-vertical-flux condition. Such a variation in the hydrostatic pressure gradient is a direct physical consequence of the rising mean temperature of the porous medium coupled with the requirement of zero mean flow. It may be viewed as a readjustment of the hydrostatic pressure due to the changing environment. Given the above expressions, (23) and (24), the long-term values of Rb above which there is no convection are given by,

$$\text{Case 1:} \quad \text{Rb} = \tfrac{1}{2}\text{Ra}, \qquad\qquad \text{Case 2:} \quad \text{Rb} = \tfrac{1}{4}\text{Ra}. \tag{29}$$

At earlier times we may calculate the values of $\theta_{\max}$ and $\theta_{\min}$ from Eqs. (21) and (22) to find the times at which convection starts, and the result of these computations are shown in Fig. 6. For a chosen value of Rb/Ra the fluid is stagnant until the appropriate curve is crossed after which convection ensues. The Figure confirms the bounds given in Eq. (29) which give the maximum values of Rb above which the fluid remains stagnant.

It is essential to determine where the yield surfaces are as a function of time. If we write those locations in terms of η, then Eq. (6) gives the following two conditions:

$$\theta(\eta_1, t) = \frac{p_x}{\text{Ra}} + \frac{\text{Rb}}{\text{Ra}}, \tag{30}$$

and

$$\theta(\eta_2, t) = \frac{p_x}{\text{Ra}} - \frac{\text{Rb}}{\text{Ra}}, \tag{31}$$

where η_1 and η_2 are the locations and where $\eta_1 < \eta_2$. The condition of zero fluid flux up the layer means that the following condition must be satisfied:

$$\int_0^{\eta_1} \left[\theta - \frac{p_x}{\mathrm{Ra}} - \frac{\mathrm{Rb}}{\mathrm{Ra}}\right] d\eta + \int_{\eta_2}^{\eta_3} \left[\theta - \frac{p_x}{\mathrm{Ra}} + \frac{\mathrm{Rb}}{\mathrm{Ra}}\right] d\eta = 0. \tag{32}$$

This becomes,

$$\begin{aligned} &2t^{1/2} \sum_{n=0}^{\infty} A_n \left[\mathrm{i}^2\mathrm{erfc}\left(\frac{n}{\sqrt{t}}\right) - \mathrm{i}^2\mathrm{erfc}\left(\eta_1 + \frac{n}{\sqrt{t}}\right) + \mathrm{i}^2\mathrm{erfc}\left(\eta_2 + \frac{n}{\sqrt{t}}\right) - \mathrm{i}^2\mathrm{erfc}\left(\eta_3 + \frac{n}{\sqrt{t}}\right)\right] \\ &-2t^{1/2} \sum_{n=0}^{\infty} B_n \left[\mathrm{i}^2\mathrm{erfc}\left(\frac{n+1}{\sqrt{t}}\right) - \mathrm{i}^2\mathrm{erfc}\left(\frac{n+1}{\sqrt{t}} - \eta_1\right) + \mathrm{i}^2\mathrm{erfc}\left(\frac{n+1}{\sqrt{t}} - \eta_2\right) - \mathrm{i}^2\mathrm{erfc}\left(\frac{n+1}{\sqrt{t}} - \eta_3\right)\right] \\ &-(\eta_1 - \eta_2 + \eta_3)\frac{p_x}{\mathrm{Ra}} - (\eta_1 + \eta_2 - \eta_3)\frac{\mathrm{Rb}}{\mathrm{Ra}} \\ &=0, \end{aligned} \tag{33}$$

where $\eta_3 = 1/(2\sqrt{t})$, which is equivalent to $y = 1$, and where the new coefficents, A_n and B_n are given by,

$$\text{Case 1:} \quad A_n = (-1)^n, \quad B_n = (-1)^{n+1}, \qquad\qquad \text{Case 2:} \quad A_n = B_n = 1. \tag{34}$$

Equations (30), (31) and (33) may be solved for η_1, η_2 and p_x/Ra using a straightforward Newton-Raphson solver and the results obtained are essentially exact to near machine accuracy.

Figures 7 and 8 show the evolution with time of the yield surface locations for a selection of values of Rb/Ra and for Cases 1 and 2, respectively. In both Figures the abscissae are $\log_{10} t$ in order to view the evolution over three orders of magnitude. In addition each Figure has two curves corresponding to each value of Rb/Ra; the channel is delineated into three regions the middle one of which is stagnant, while the one neighbouring the hot (cold) surface corresponds to upward (downward) flow. Thus, in Fig. 7 and for Rb/Ra, the whole channel is stagnant until $t = 0.0078540$ (i.e. $\log_{10} t = -2.10491$) after which the centreline of the stagnant plug moves rapidly towards the heated surface and then moves back towards the centre of the channel. For larger values of Rb/Ra the initial movement of the centre of the plug becomes less rapid, but in all cases the yield surfaces are symmetrically placed about $y = \frac{1}{2}$ when t is sufficiently large. More specifically they are located at

$$y = \tfrac{1}{2} \pm \frac{\mathrm{Rb}}{\mathrm{Ra}}. \tag{35}$$

This Figure also shows clearly the increasing delay before convection sets in as Rb/Ra increases.

In Fig. 8 it is clear that there is almost no difference between Cases 1 and 2 at early times, and while the yield surfaces move more quickly to their ultimate positions within the channel for Case 2 when compared with Case 1, they are no longer located symmetrically about the centreline since the temperature profile is quadratic rather than linear.

Figures 9 and 10 display information on how the hydrostatic gradient varies with time. For Case 1, which is shown in Fig. 9, we show the variation of p_x. For each value of Rb/Ra the value of p_x is precisely equal to Rb/Ra, and this arises because Eq. (26) must be satisfied and $\theta_{\min} = 0$. As the mean temperature in the channel rises so does the hydrostatic pressure gradient, and eventually it tends towards 1/2Ra. On the other hand such a simple analysis for Case 2 cannot be made because $\theta_{\min}$ is no longer zero, but eventually rises linearly with time. As the overall temperature profile continues to rise, so does the value of p_x, and therefore we have plotted the evolution with time of $(p_x - t)/\mathrm{Ra}$ in Fig. 10.

Finally, we turn to the induced velocity within the layer, and Figs. 11 and 12 show how the maximum and minimum velocities (which correspond to the boundaries, $y = 0$ and $y = 1$, respectively) vary with time. For both cases we see clearly that flow up the heated surface is greater in magnitude than the flow down the other surface soon after convection begins. And, for relatively small values of Rb/Ra, the initial velocity of the flow down the cooler wall is much weaker than its warmer counterpart. As time progresses $u_{\max}$ and

$u_{\min}$ tend towards the same magnitude for Case 1, which again reflects the symmetry of the final velocity profile. There remains a distinct asymmetry at late times for the Case 2 profiles. In these Figures we have also included the corresponding curves for Newtonian fluids for comparison.

5 Conclusions

We have studied the effect of the presence of a yield threshold on convection which is induced by suddenly heating a vertical surface bounding a porous medium with a uniform heat flux. Three cases were considered, namely a infinitely wide domain, and two different channels which are distinguished by having either a fixed cold temperature or an insulated boundary condition.

The temperature profile evolves in time in a manner which is independent of any fluid flow and these have been presented. By virtue of the fact that heat is being supplied contiuously to the porous medium the fluid remains stagnant at early times because the resulting buoyancy forces are too weak to overcome the yield threshold.

For the infinite domain convection will always happen eventually since the boundary temperature is proportional to $t^{1/2}$ and therefore buoyancy forces also rise without limit. On the other hand convection will arise only if $\mathrm{Rb} < \frac{1}{2}\mathrm{Ra}$ for Case 1 and if $\mathrm{Rb} < \frac{1}{4}\mathrm{Ra}$ for Case2. These results are somewhat different from those obtained in Rees and Bassom (2015) where the analogous cases were considered where the heated surface was held at a fixed temperature (though not the equivalent of the present Case 2). There it was found that there is a restriction on the value of Rb/Ra even for the infinite domain. It was also found that convection, if it does arise, will begin immediately.

Acknowledgement

The authors would like to thank the anonymous reviewers for their comments which have served to improve our paper.

References

[1] D.A.S. Rees, Convection of a Bingham fluid in a porous medium. Chapter 17. Handbook of Porous Media Volume III (ed. K.Vafai) Taylor and Francis (2015).

[2] W.J. Yang, H.C. Yeh, Free convective flow of Bingham plastic between two vertical plates, Trans. A.S.M.E. Journal of Heat Transfer **87(2)** (1965) 319-320.

[3] Y. Bayazitoglu, P.R. Paslay, P. Cernocky, Laminar Bingham fluid flow between vertical parallel plates, International Journal of Thermal Sciences **46** (2007) 349-35.

[4] N. Patel, D.B. Ingham, Analytic solutions for the mixed convection flow of non-Newtonian fluids in parallel plate ducts, International Communcations in Heat Mass Transfer **21(1)** (1994) 75-84.

[5] A. Barletta, E. Magyari, Buoyant Couette-Bingham flow between vertical parallel plates, International Journal of Thermal Sciences **47** (2008) 811-819.

[6] I. Karimfazli, I.A. Frigaard, Natural convection flows of a Bingham fluid in a long vertical channel, Journal of Non-Newtonian Fluid Mechanics **201** (2013) 39-55.

[7] J. Kleppe, W.J. Marner, Transient free convection in a Bingham plastic on a vertical flat plate, Trans. A.S.M.E., Journal of Heat Transfer **94(4)** (1972) 371-376.

[8] D.A.S. Rees, A.P. Bassom, Unsteady thermal boundary layer flows of a Bingham fluid in a porous medium, International Journal of Heat and Mass Transfer **82** (2015) 460-467.

[9] H. Pascal, Nonsteady flow through porous media in the presence of a threshold gradient, Acta Mechanica **39** (1981) 207–224.

Appendix

The aim here is to solve (17) for $\eta_{\rm y}$ for large values of t. Using the substitution (18), Eq.(17) becomes,

$$\frac{2}{\sqrt{\pi}}e^{-\eta_{\rm y}^2} - 2\eta_{\rm y}\,\mathrm{erfc}\,\eta_{\rm y} = \frac{1}{\sqrt{\tau}}. \tag{36}$$

We omit the details of our analysis, which follows closely that of [8], we eventually obtain the following series:

$$\eta_{\rm y} = \delta^{-1/2}\Big[1 + (\tfrac{1}{2}\mathcal{D})\delta - \tfrac{1}{8}(\mathcal{D}^2 + 4\mathcal{D} + 6)\delta^2 + \tfrac{1}{16}(\mathcal{D}^3 + 8\mathcal{D}^2 + 26\mathcal{D} + 33)\delta^3 + \cdots\Big]. \tag{37}$$

Evaluation of the scaled mass flux given in Eq. (19) requires the evaluation of $\mathrm{erf}\,\eta_{\rm y}$. We find that,

$$Q/t = 1 - \frac{1}{2(\tau\delta)^{1/2}}\Big[2 + (\mathcal{D}+2)\delta - (\tfrac{1}{4}\mathcal{D}^2 + 2\mathcal{D} + \tfrac{9}{2})\delta^2 + \cdots\Big]. \tag{38}$$

In these two expressions we have defined δ and $\mathcal{D}$ according to

$$e^{-1/\delta} = \sqrt{\frac{\pi}{\tau}} \qquad \Big(\text{ or } \quad \delta = 2/\ln(\tau/\pi)\ \Big) \qquad \text{and} \qquad \mathcal{D} = \ln\delta. \tag{39}$$

Figures

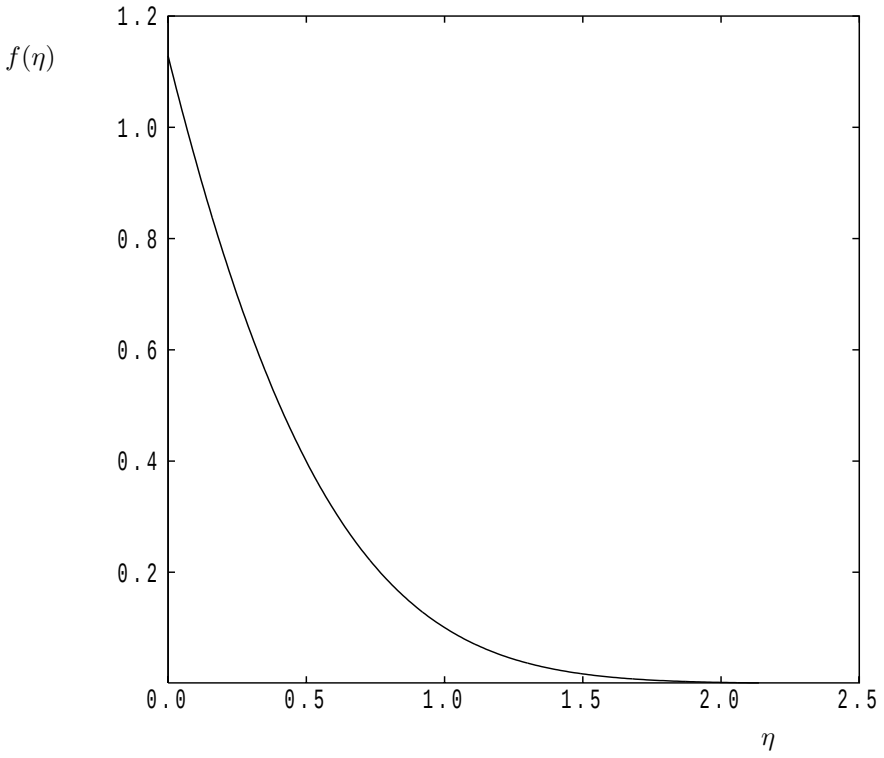

Figure 1: Showing the self-similar temperature profile, $f(\eta)$, for the infinite domain.

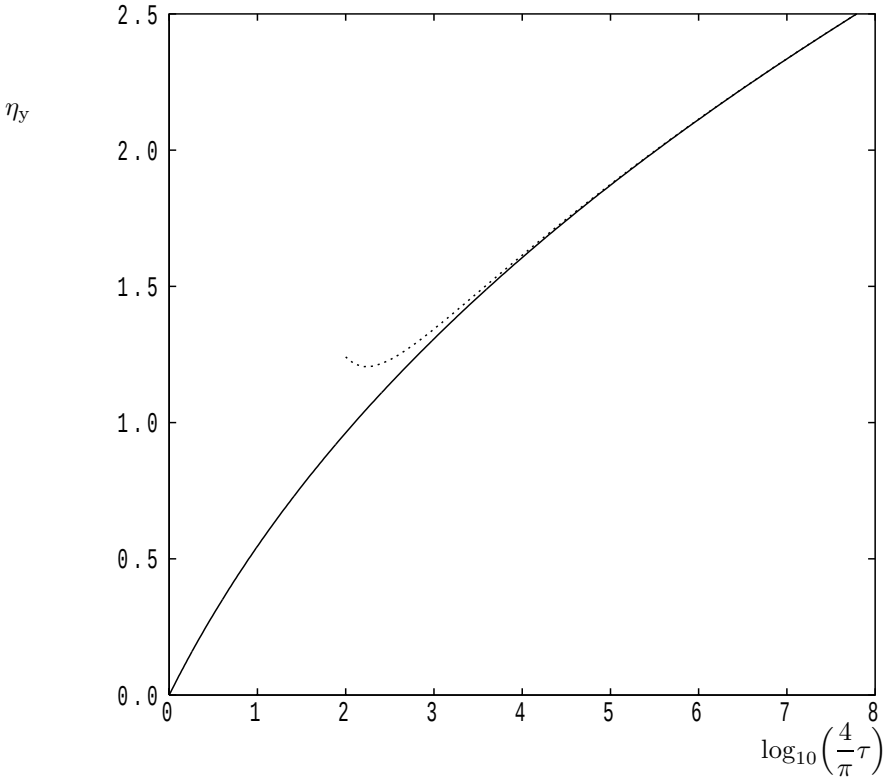

Figure 2: The variation in the location of the yield surface for the infintie domain.

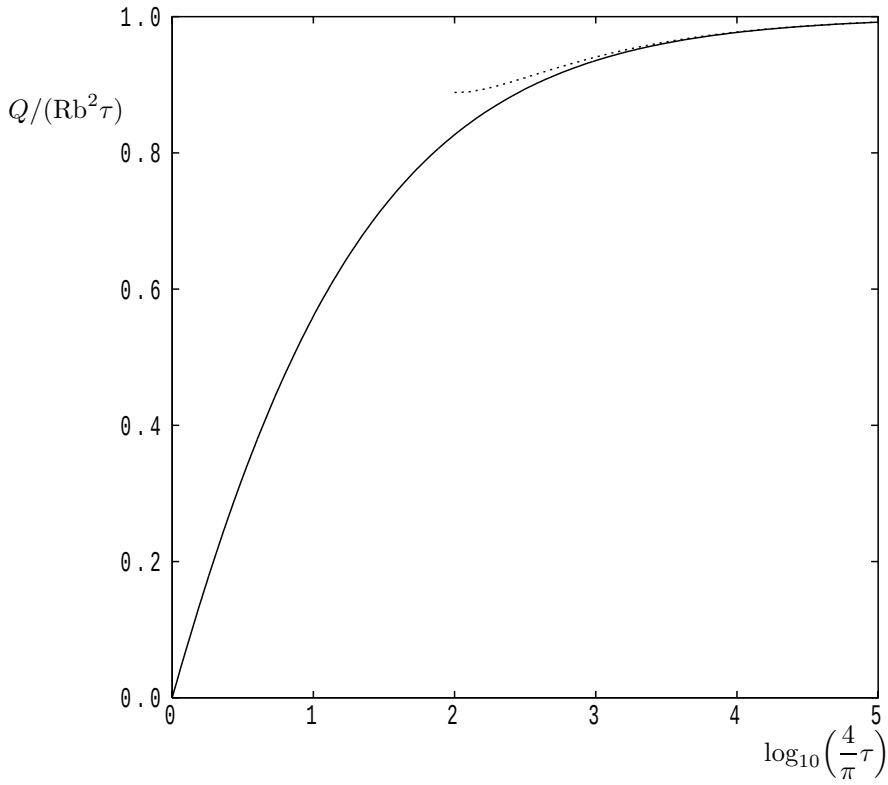

Figure 3: The variation in a scaled total mass flux with time for the infinite domain.

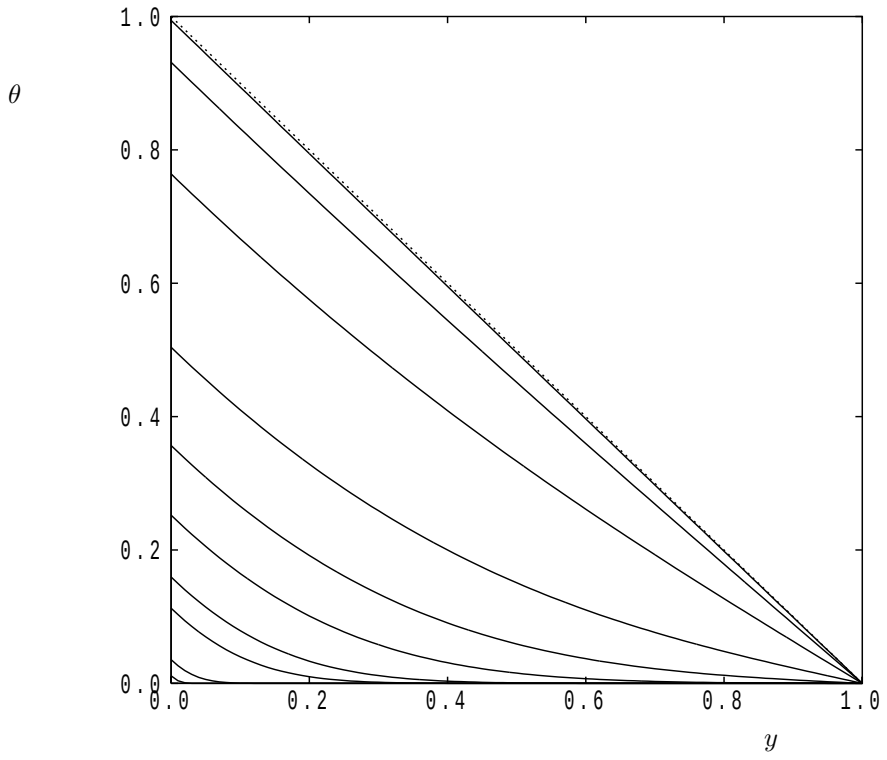

Figure 4: Temperature profiles for the tall channel (Case 1) at $t = 0.0001$, 0.001, 0.01, 0.02, 0.05, 0.1, 0.2, 0.5, 1, 2, and as $t \to \infty$ (dotted line).

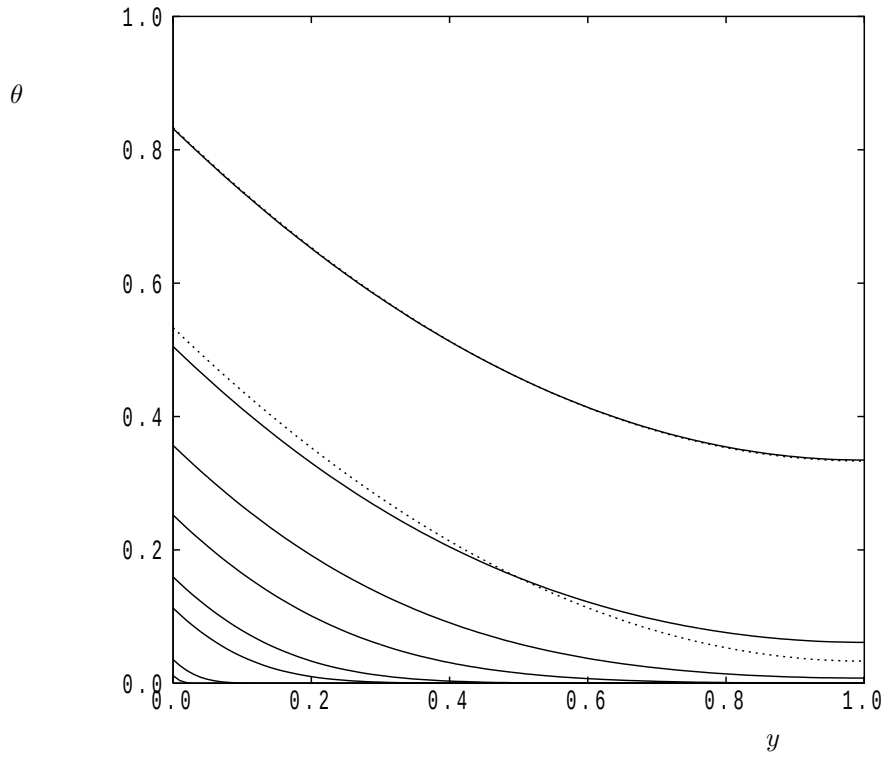

Figure 5: Temperature profiles for the tall channel (Case 2) at $t = 0.0001$, 0.001, 0.01, 0.02, 0.05, 0.1, 0.2 and 0.5. Also shown as dotted lines are the large-t profiles given by Eqs. (23) and (24) but evaluated at $t = 0.2$ and 0.5.

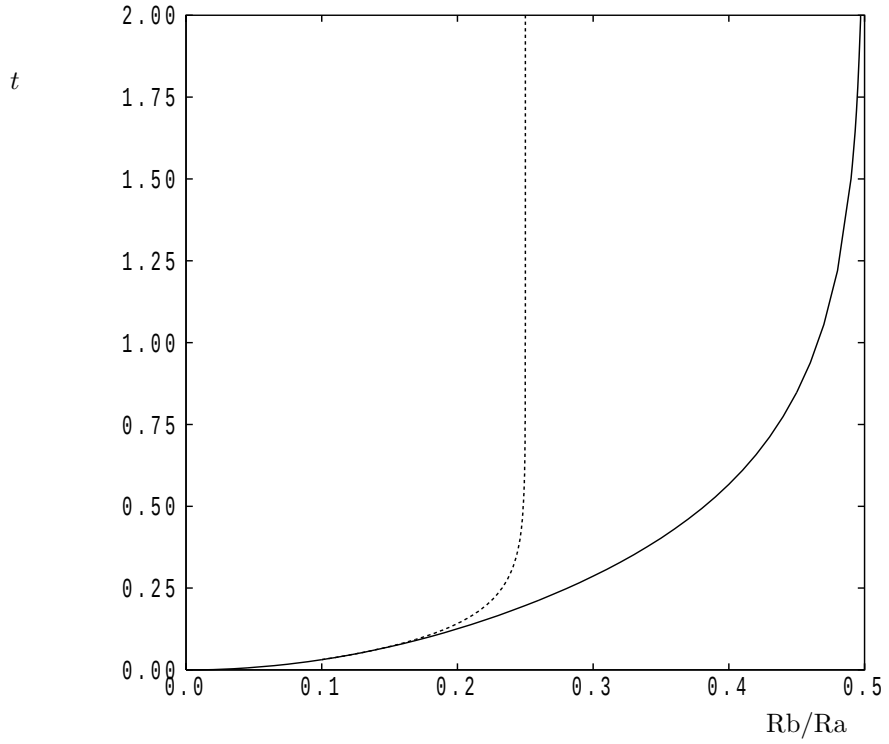

Figure 6: Showing the time at which convection first arises; points below the curves correspond to stagnant fluid. Case 1 corresponds to teh continuous line and Case 2 to the dotted line.

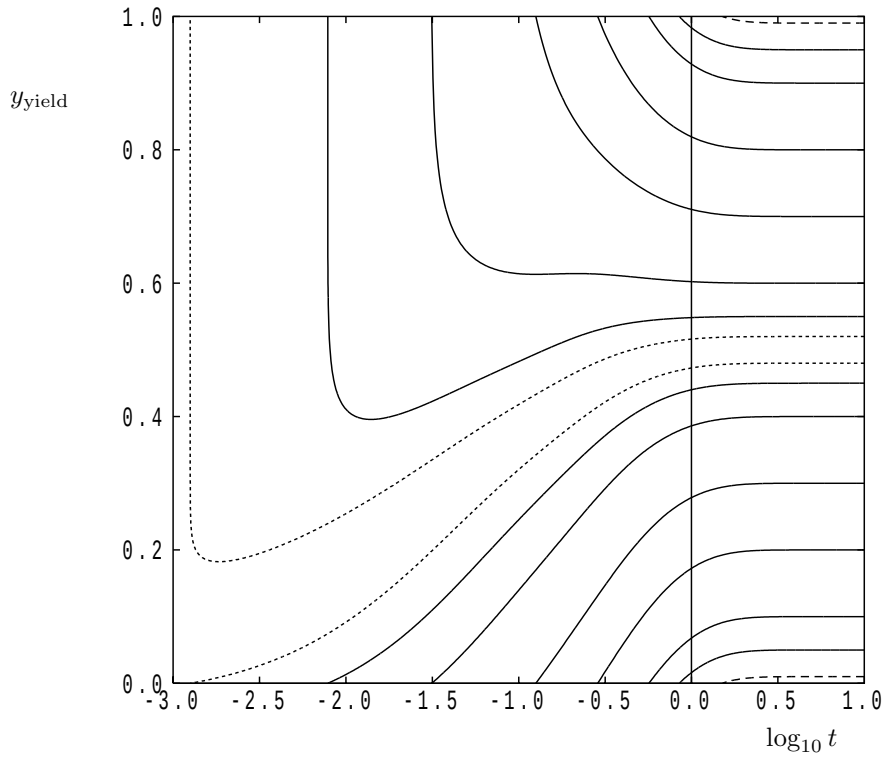

Figure 7: Locations of the yield surfaces as functions of time for Rb/Ra = 0.02 (dotted lines), 0.05, 0.1, 0.2, 0.3, 0.4, 0.45 and 0.49 (dashed lines). Each value of Rb has two yield surfaces, and the fluid is stationary between these two surfaces. Case 1.

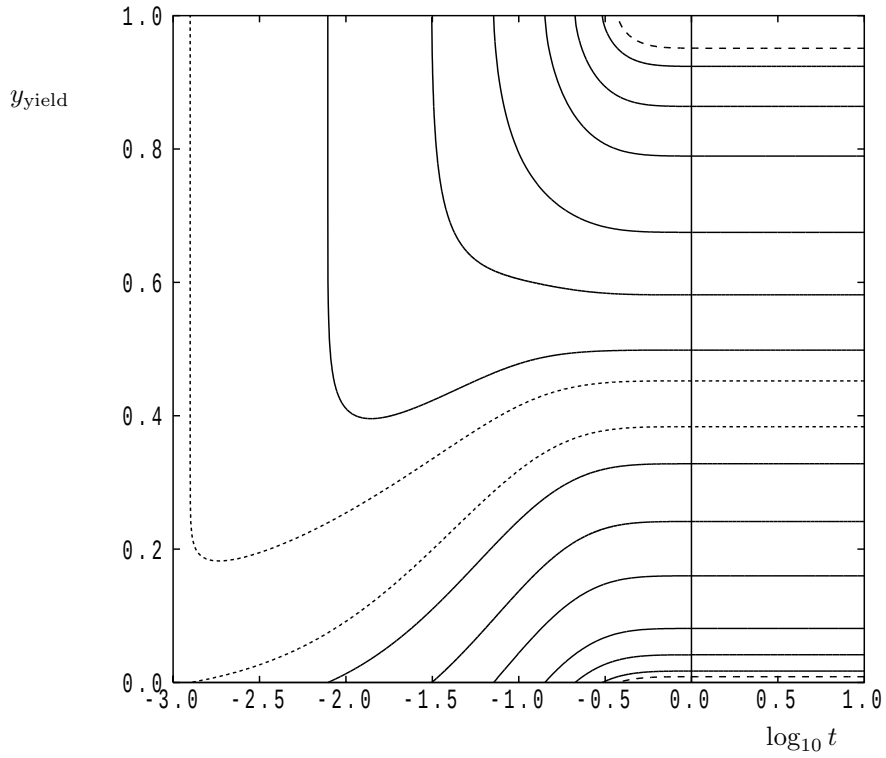

Figure 8: Locations of the yield surfaces as functions of time for Rb/Ra = 0.02 (dotted lines), 0.05, 0.1, 0.15, 0.2, 0.225, 0.24 and 0.245 (dashed lines). Each value of Rb has two yield surfaces, and the fluid is stationary between these two surfaces. Case 2.

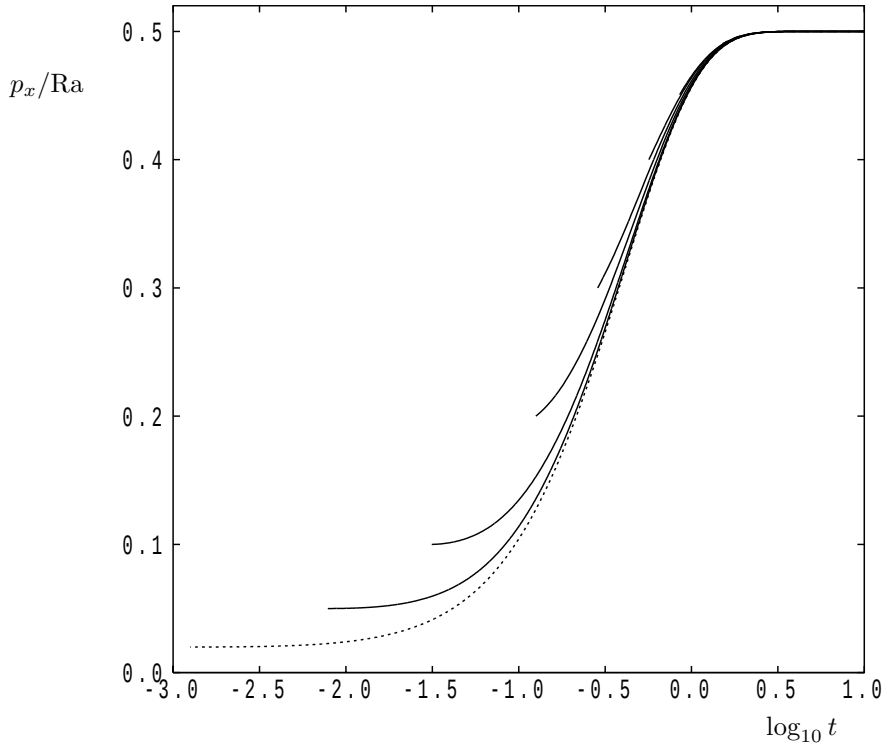

Figure 9: Variation with time of the value of p_x/Ra; for Rb/Ra = 0.02 (dotted line), 0.05, 0.1, 0.2, 0.3, 0.4 and 0.45 (dashed line).

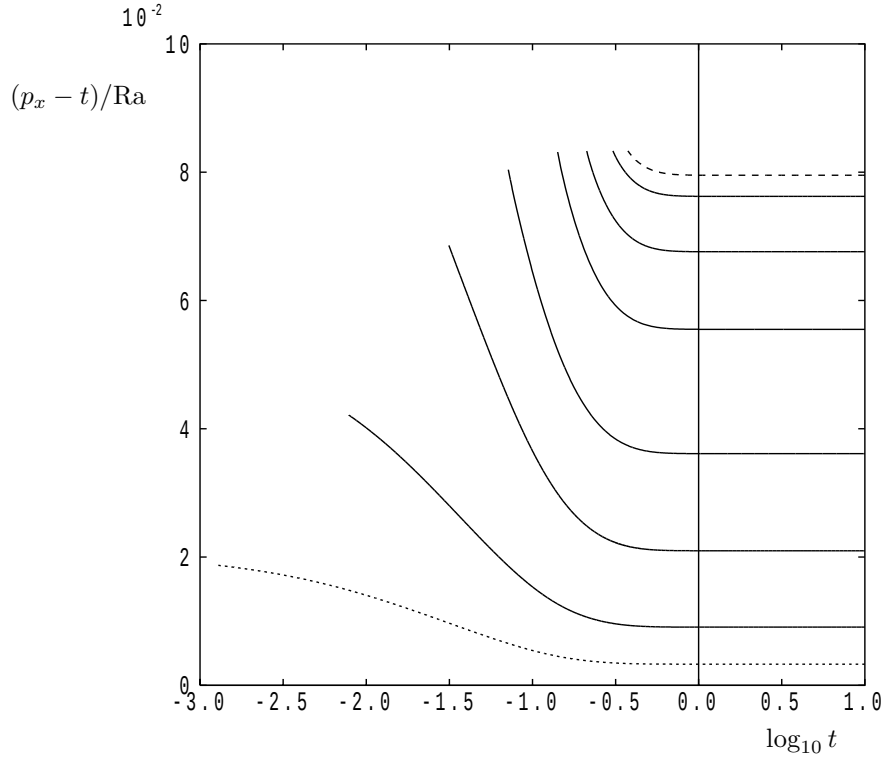

Figure 10: Variation with time of the value of $(p_x - t)$/Ra; for Rb/Ra = 0.02 (dotted line), 0.05, 0.1, 0.15, 0.2, 0.225, 0.24 and 0.245 (dashed line).

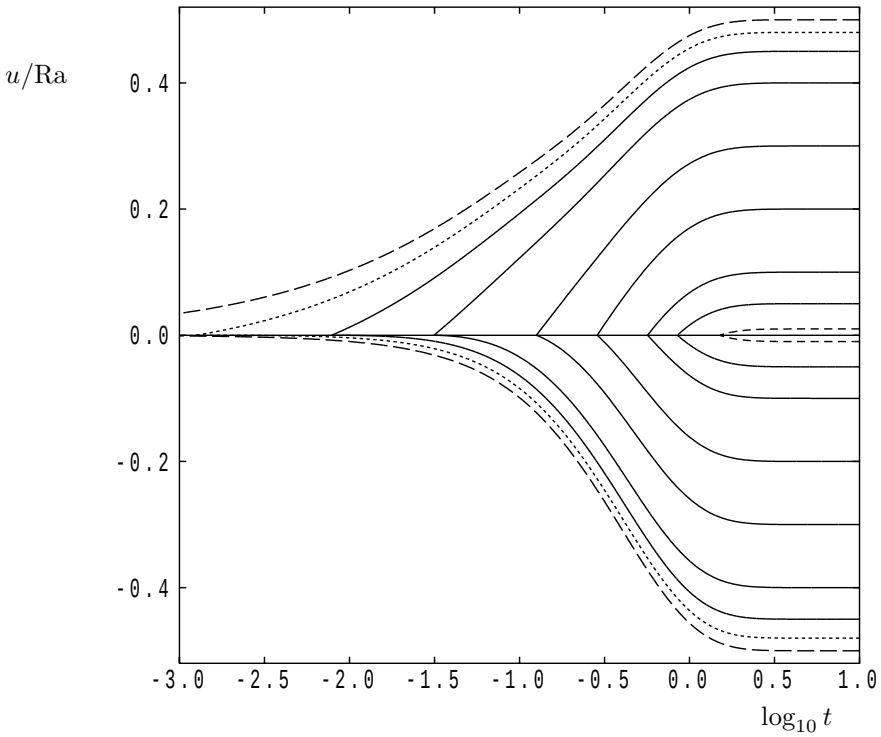

Figure 11: Variation with time of the maximum and minimum fluid velocities for Rb/Ra = 0 (dashed line) 0.02 (dotted lines), 0.05, 0.1, 0.2, 0.3, 0.4, 0.45 and 0.49 (short dashes). Curves which lie above the line, $u = 0$, represent the maxima while those below represent the minima. Case 1.

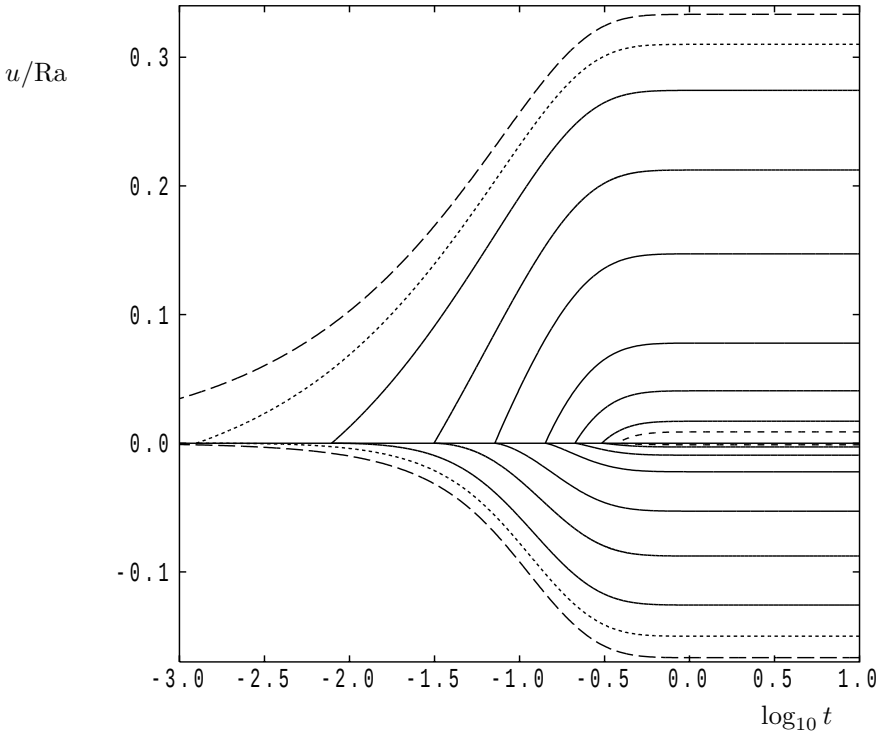

Figure 12: Variation with time of the maximum and minimum fluid velocities for Rb/Ra = 0 (dashed line) 0.02 (dotted lines), 0.05, 0.1, 0.15, 0.2, 0.225, 0.245 and 0.245 (short dashes). Curves which lie above the line, $u = 0$, represent the maxima while those below represent the minima. Case 2.